学位論文

NSUN3-mediated mitochondrial tRNA 5-formylcytidine modification is essential for embryonic development and respiratory complexes in mice
（NSUN3 によるミトコンドリア tRNA の 5-ホルミルシチジン修飾はマウスの胎児発育と呼吸鎖複合体に必須である）

村上　慶高

Yoshitaka　Murakami

指導教員

富澤　一仁　教授

熊本大学大学院医学教育部博士課程医学専攻分子生理学

2023年度

学　位　論　文

論文題名　：　**NSUN3-mediated mitochondrial tRNA 5-formylcytidine modification is essential for embryonic development and respiratory complexes in mice**

（NSUN3 によるミトコンドリア tRNA の 5-ホルミルシチジン修飾はマウスの胎児発育と呼吸鎖複合体に必須である）

著 者 名　：　村　上　慶　高

Yoshitaka Murakami

指導教員名　：　熊本大学大学院医学教育部博士課程医学専攻分子生理学 富澤　一仁　教授

審査委員名　：　小児科学担当教授　中村　公俊

幹細胞ストレス学担当教授　滝澤　仁

心臓発生学担当特任准教授　有馬　勇一郎

細胞医学担当講師　古賀　友紹

2023年度

NSUN3-mediated mitochondrial tRNA 5-formylcytidine modification is essential for embryonic development and respiratory complexes in mice

Yoshitaka Murakami[1,2], Fan-Yan Wei[3], Yoshimi Kawamura[4], Haruki Horiguchi[5], Tsuyoshi Kadomatsu[5], Keishi Miyata[5], Kyoko Miura[4,6], Yuichi Oike[5,6], Yukio Ando[7], Mitsuharu Ueda[2,6], Kazuhito Tomizawa[1,6,*] and Takeshi Chujo[1,*]

[1]Department of Molecular Physiology, Faculty of Life Sciences, Kumamoto University, Kumamoto 860-8556, Japan.

[2]Department of Neurology, Faculty of Life Sciences, Kumamoto University, Kumamoto 860-8556, Japan.

[3]Department of Modomics Biology and Medicine, Institute of Development, Aging and Cancer, Tohoku University, Sendai 980-8575, Japan.

[4]Department of Aging and Longevity Research, Faculty of Life Sciences, Kumamoto University, Kumamoto 860-0811, Japan.

[5]Department of Molecular Genetics, Faculty of Life Sciences, Kumamoto University, Kumamoto 860-8556, Japan.

[6]Center for Metabolic Regulation of Healthy Aging, Kumamoto University, Kumamoto,860-8556, Japan.

[7]Department of Amyloidosis Research, Faculty of Pharmaceutical Sciences, Nagasaki International University, Sasebo 859-3298, Japan.

* To whom correspondence should be addressed:

Takeshi Chujo
Tel: +81-96-373-5051
Email: tchujo@kumamoto-u.ac.jp

Kazuhito Tomizawa
Tel: +81-96-373-5050
Email: tomikt@kumamoto-u.ac.jp

Abstract

In mammalian mitochondria, translation of the AUA codon is supported by 5-formylcytidine (f^5C) modification in the mitochondrial methionine tRNA anticodon. The 5-formylation is initiated by NSUN3 methylase. Human *NSUN3* mutations are associated with mitochondrial diseases. Here we show that *Nsun3* is essential for embryonic development in mice with whole-body *Nsun3* knockout embryos dying between E10.5 and E12.5. To determine the functions of NSUN3 in adult tissue, we generated heart-specific *Nsun3* knockout (*Nsun3*^{HKO}) mice. *Nsun3*^{HKO} heart mitochondria were enlarged and contained fragmented cristae. *Nsun3*^{HKO} resulted in enhanced heart contraction and age-associated mild heart enlargement. In the *Nsun3*^{HKO} hearts, mitochondrial mRNAs that encode respiratory complex subunits were not down regulated, but the enzymatic activities of the respiratory complexes decreased, especially in older mice. Our study emphasizes that mitochondrial tRNA anticodon modification is essential for mammalian embryonic development and shows that tissue-specific loss of a single mitochondrial tRNA modification can induce tissue aberration that worsens in later adulthood.

Introduction

tRNA molecules function as adaptors that convert genetic information transcribed in the form of mRNA into proteins[1,2]. tRNAs contain a variety of modified nucleosides that are post-transcriptionally incorporated by specific enzymes. These tRNA modifications play pivotal roles in maintaining tRNA structural integrity, biochemical stability and codon-anticodon interactions[3,4]. The physiological importance of tRNA modifications is shown by the presence of more than 50 human tRNA modification enzymes whose mutations or expressional aberrations are associated with diseases that frequently manifest as brain dysfunction, cancer, diabetes, or mitochondrial diseases[3-5].

In humans, protein synthesis takes place not only in the cytoplasm, but also within mitochondria, where 13 respiratory complex proteins are synthesized by translation of mRNAs using 22 tRNAs and two ribosomal RNAs (rRNAs) transcribed from mitochondrial DNA (mt-DNA)[6]. The 22 human mt-tRNAs contain 18 kinds of modifications at 137 positions[7], many of which are important for health. Mitochondrial disease collectively refers to a group of diseases caused by mitochondrial dysfunction. Mitochondrial disease-associated mutations have been reported in several nucleus-encoded mt-tRNA modification enzyme genes[8-14], suggesting that mt-tRNA modifications play pivotal roles in intra-mitochondrial protein synthesis.

Moreover, whole-body knockouts (KO) of the mt-tRNA modification enzyme genes *Mto1* or *Mtu1* are embryonic lethal in mice[15,16]. *Mto1* encodes a mt-tRNA modification enzyme required for synthesis of 5-taurinomethyluridine (τm^5U) at the anticodon first nucleotide in five mt-tRNAs (mt-tRNA^{Leu1}, mt-tRNA^{Trp}, mt-tRNA^{Gln}, mt-tRNA^{Lys} and mt-tRNA^{Glu}). *Mtu1* encodes a mt-tRNA modification enzyme that introduces thiolation to three τm^5U-containing mt-tRNAs, resulting in τm^5s^2U modification at the

anticodon first nucleotide of three mt-tRNAs (mt-tRNA^{Gln}, mt-tRNA^{Lys} and mt-tRNA^{Glu}). In contrast to embryonic lethality in mice lacking *Mto1* or *Mtu1* which encode enzymes that target the first nucleotide of mt-tRNA anticodon, reported mice lacking enzymes that target other regions of mt-tRNAs are viable. For example, mice lacking *Cdk5rap1*, which encodes an enzyme that methyl-thiolates the nucleotide adjacent to the mt-tRNA anticodon are viable[17]. Additionally, mice lacking *NOL1/NOP2/Sun domain family member 2* (*Nsun2*), which encodes a methyltransferase that targets the variable loop of mitochondrial and cytoplasmic tRNAs[18,19], are viable and do not display an apparent mitochondria-related phenotype[18,20].

The human mitochondrial genetic code deviates from the canonical cytoplasmic genetic code. For example, the AUA codon, which encodes isoleucine in cytoplasmic translation, encodes methionine in mitochondria. To decode AUA as methionine, mt-tRNA^{Met} contains a 5-formylcytidine (f^{5}C) modification in the anticodon first nucleotide[21] (Figure 1a, b). f^{5}C enables the mt-tRNA^{Met} anticodon (CAU) to base pair with not only the AUG codon but also with the AUA codon[22]. f^{5}C enables f^{5}C-A pairing via imino-oxo tautomerization of the cytosine base, which is stabilized by the 5-formyl group[23]. f^{5}C is synthesized by two mitochondrial matrix-localized enzymes, NSUN3 and AlkB homolog 1 (ALKBH1). After mt-tRNA^{Met} is transcribed, NSUN3 first methylates cytidine to form 5-methylcytidine, and ALKBH1 then oxidizes the methyl group to form a formyl group[24-27]. Due to the importance of f^{5}C in mitochondrial translation, knockout of *NSUN3* or *ALKBH1* in cultured human cells, as well as mutation of *Nsun3* in mouse embryonic stem cells, result in a strong reduction of mitochondrial protein synthesis[25,26,28].

Mitochondrial disease-associated mutations have been found in several nucleus-encoded mt-tRNA modification enzyme genes, such as *MTO1*, *GTPBP3*, *MTU1*,

TRMT10C, *PUS1* and *TRMT5*[8-12,14]. The mutations result in dysfunctions and developmental disorders in highly energy consuming organs including the heart, skeletal muscle, liver and brain. Similar to the cases of other important mt-tRNA modification enzymes, mutations in the *NSUN3* gene are associated with mitochondrial diseases. One mitochondrial disease patient, who had compound heterozygous *NSUN3* mutations, developed symptoms of the disease at the age of three months including muscle weakness, ophthalmoplegia, convergence nystagmus, increased plasma lactate level, microcephaly and developmental delay[13]. Another mitochondrial disease patient with different compound heterozygous *NSUN3* mutations presented at the age of four months with muscle weakness, hypotonia, lactic acidosis, global developmental delay and seizures[29]. In addition, a hypertension patient harboring a point mutation in the *mt-tRNA^{Met}* (A4435G in mtDNA) had thickening of his heart left ventricle posterior wall during his 60s and 70s[30]. This mutation corresponds to the 3' adjacent nucleotide to the anticodon of mt-tRNA^{Met} (position 37 in the conventional tRNA position numbering) and has been found to decrease the efficiency of NSUN3-mediated mt-tRNA^{Met} modification in vitro[26].

To investigate the physiological functions of NSUN3-mediated f^{5}C modification, we generated *Nsun3* KO mice. Whole-body *Nsun3* KO mice were embryonic lethal, highlighting the importance of NSUN3 along with MTO1 and MTU1 as essential mt-tRNA anticodon modification enzymes for mouse embryonic development. These results establish that mt-tRNA anticodon modifications are crucial for mammalian embryonic development. Moreover, we showed that heart-specific *Nsun3* KO resulted in impaired heart respiratory complex activities and mild heart aberration especially at older age, indicating that tissue-specific loss of a single tRNA modification species in a single mt-

tRNA can cause tissue aberration especially in later adulthood.

Results

Nsun3 is essential for embryonic development in mice

To investigate the physiological importance of NSUN3, we first attempted to generate whole-body *Nsun3* KO mice by crossing transgenic mice having exon 4 of *Nsun3* gene floxed by LoxP sequence (*Nsun3*$^{Flox/Flox}$) with transgenic mice carrying Cre recombinase under control of cytomegalovirus enhancer and chicken *β-actin* (CAG) promoter. This resulted in permanent deletion of targeted exons in the germ cells. The resulting *Nsun3*$^{(Flox/-);CAGcre}$ mice were further crossed to C57BL/6J mice to yield *Nsun3* heterozygous mice (*Nsun3*$^{+/-}$). By mating *Nsun3*$^{+/-}$ mice, we obtained five wild-type mice and 13 heterozygous mice, with no homozygous *Nsun3* KO mice obtained after multiple generations of breeding (Figure 1c). We examined the morphology of embryos at embryonic day (E) 12.5 (Figure 1d, 1e; Supplementary Figure 1a). While the morphology of *Nsun3* heterozygous embryos did not differ from wild-type embryos, *Nsun3* KO embryos were small and appeared to start to become absorbed into mother's uterus. At E10.5, while *Nsun3* KO embryos were smaller in comparison to wild-type or heterozygous embryos (Figure 1f), heart beats were observed in all *Nsun3* KO embryos. Thus, *Nsun3* KO embryos are alive at E10.5 but die before E12.5. These results clearly indicate that constitutive *Nsun3* deficiency leads to embryonic lethality in mice.

Phenotypes in heart-specific *Nsun3* knockout mice

To clarify the possible roles of NSUN3-mediated tRNA f^5C modification in adult tissue,

we generated heart-specific *Nsun3* knockout (*Nsun3*^{HKO}) mice. We chose to ablate *Nsun3* in the heart because heart and skeletal muscle are the most susceptible tissues to mitochondrial dysfunction[31]. Another reason for choosing heart is that a hypertension patient having a *mt-tRNA*^{Met} mutation that can reduce NSUN3-mediated modification of mt-tRNA^{Met}, showed left ventricle posterior wall thickening during his 60s and 70s[26,30].

Nsun3^{HKO} mice were generated by crossing transgenic mice harboring exon four of the *Nsun3* gene floxed by LoxP sequences (*Nsun3* Flox mice) with transgenic mice expressing Cre recombinase under the control of heart-specific Myosin heavy chain promoter (Myh6-Cre mice) (Figure 2a). The *Nsun3*^{HKO} mice grew up without any obvious morphological defects, and adult *Nsun3*^{HKO} mice had equivalent body weights compared to the Flox mice (Figure 2b). Heart muscle cell-specific *Cre* expression from the *Myh6* promoter resulted in removal of most of *Nsun3* gene exon 4 in the heart, as confirmed by reverse-transcription quantitative PCR (RT-qPCR) (Figure 2c). A small fraction of the remaining exon 4 in *Nsun3*^{HKO} heart may derive from non-heart muscle cells (e.g., blood vessel cells). Mass spectrometry analysis of heart total RNA nucleosides confirmed that f^{5}C was absent in *Nsun3*^{HKO} hearts (Figure 2d).

To investigate the impact of *Nsun3* deficiency on the heart, we first measured the mass of dissected hearts in 14-week-old young adult mice and 50-week-old mice (Figure 3a). Although the *Nsun3*^{HKO} hearts showed equivalent weight as the control Flox mice at 14 weeks of age, *Nsun3*^{HKO} hearts were 31% heavier than Flox mice hearts at 50 weeks of age. Thus, at older age, *Nsun3*^{HKO} hearts show mild enlargement, which often occurs as a compensatory response to compromised heart function.

To monitor heart function, we performed cardiac ultrasonography (Figure 3b, c). The relative masses of the left ventricles, estimated by ultrasonography, were normal

in 14-week-old, young adult *Nsun3*^{HKO} mice, but showed slightly larger tendency in 50-week-old *Nsun3*^{HKO} mice, although the difference was statistically insignificant (Figure 3d). On the other hand, left ventricle volume decreased in the systolic phase of *Nsun3*^{HKO} hearts at 14 weeks (Figure 3e). Accordingly, although statistically insignificant, the ejection fraction showed an increasing tendency in *Nsun3*^{HKO} mice hearts (Figure 3f). In addition, the left ventricle thickness increased in the systolic phase of 50-week-old *Nsun3*^{HKO} heart (Figure 3g), suggesting enhanced heart contraction. Collectively, our results demonstrate that heart *Nsun3* knockout causes the development of mild heart abnormalities that became more apparent at older age.

Aberrant mitochondrial morphology in *Nsun3*^{HKO} mouse heart

Abnormal mitochondrial morphology is a hallmark of mitochondrial dysfunction. Since NSUN3 is a mt-tRNA^{Met} modification enzyme required for efficient mitochondrial translation[13,24,26], we next examined mitochondrial morphology using transmission electron microscopy. Mitochondria in the cardiac muscle of Flox control mice were filled with well-organized, elongated cristae structures (Figure 4a). By contrast, the *Nsun3*^{HKO} heart mitochondria had fragmented cristae structures (Figure 4b). Metabolic needs due to impairment of mitochondrial function can promote mitochondrial remodeling as a compensation mechanism[32,33]. Indeed, quantification of the mitochondrial size revealed that the mean size of *Nsun3*^{HKO} heart mitochondria (1.011 μm^2) was 1.5 times larger than the mean size of Flox heart mitochondria (0.690 μm^2) at 14 weeks of age and 1.7 times larger at 50 weeks of age (Flox: 0.685 μm^2, *Nsun3*^{HKO}: 1.174 μm^2) (Figure 4a-d). In addition, 50-week-old *Nsun3*^{HKO} heart mitochondria were 17% larger than 14-week-old

Nsun3^{HKO} heart mitochondria (Figure 4d). These aberrant mitochondrial morphologies indicated that *Nsun3*^{HKO} mice may have dysfunctional heart mitochondria.

Nsun3^{HKO} does not decrease the steady-state levels of heart mitochondrial tRNAs and mRNAs

Mitochondrial RNAs are transcribed as polycistronic precursors and then processed into each RNA species[6,34] (Figure 5a), and the stability of mature mt-RNAs is post-transcriptionally regulated by RNA-binding proteins and RNases in mitochondria[35]. To evaluate the effects of *Nsun3* loss on mitochondrial RNA steady-state levels, we conducted northern blots of heart mt-tRNAs and mt-mRNAs. As a result, we observed a slight increase in the steady-state levels of all monitored mt-tRNAs and mt-mRNAs, including mt-tRNA^{Met} (Figure 5b, c, d, e and Supplementary Figure 2). This result indicates that mt-tRNA^{Met} steady-state level increased likely due to increased mitochondrial volume (Figure 4) and/or mitochondria-wide RNA upregulation, rather than an event specific to mt-tRNA^{Met}. The mt-*Nd2* mRNA is directly connected to mt-tRNA^{Met} within the polycistronic precursor (Figure 5a). To assess whether the loss of f^{5}C modification in mt-tRNA^{Met} affects processing at the mt-tRNA^{Met}-*Nd2* boundary, the entire membrane of mt-*Nd2* northern blot is shown in Figure 5d. We observed only some increase of the precursor RNA (faint bands observed above mature mt-*Nd2*) at a comparable level to the increase in mature mt-*Nd2* mRNA level, which suggests that the loss of f^{5}C modification in mt-tRNA^{Met} has a minimal or no effect on mt-tRNA^{Met}-*Nd2* boundary processing. Overall, these results indicate that *Nsun3*^{HKO} does not decrease the steady-state levels of observed mature mt-tRNAs and mt-mRNAs.

Nsun3^{HKO} causes mitochondrial respiratory complex dysfunction exacerbated at older age

We next evaluated the quantity and activities of mitochondrial respiratory complexes in 14- and 50-week-old mice hearts. To quantify respiratory complexes, mitochondria were fractionated from 14- and 50-week-old mice hearts and whole respiratory complexes detected by blue native PAGE. In *Nsun3*^{HKO} heart mitochondria, we observed a decrease of complex IV in 14-week-old or 50-week-old heart mitochondria (Figure 6a, b, Supplementary Figure 1b). Accordingly, the steady-state level of MT-CO1 protein, a mt-DNA-encoded complex IV protein, was markedly decreased in *Nsun3*^{HKO} mice (Figure 6c, Supplementary Figure 1c, d). By contrast, the steady-state levels of mt-mRNAs, including mRNAs of all of the mtDNA-encoded complex IV proteins (mt-*Co1*, mt-*Co2* and mt-*Co3* mRNAs), were not decreased (Figure 5c), consistent with the role of NSUN3-mediated tRNA^{Met} modification in translation of mt-mRNAs rather than their stability. In the *Nsun3*^{HKO} hearts, we observed a mild increase of lactate levels (Figure 6d), which may indicate that glycolysis activity was enhanced, possibly in response to decreased respiratory complex activity in the *Nsun3*^{HKO} hearts. Thus, finally, we measured the respiratory complex activities of 14- and 50-week-old heart mitochondria. The 14-week-old, young adult *Nsun3*^{HKO} heart mitochondria showed a decrease in complex IV activity (Figure 6e). Moreover, 50-week-old *Nsun3*^{HKO} heart mitochondria showed an additional decrease in complex I activity compared to 14-week-old *Nsun3*^{HKO} (as seen by comparing Figure 6e and 6f, $P = 0.037$, Welch's t-test). Thus, *Nsun3*^{HKO} causes dysfunction of specific mitochondrial respiratory

complexes, and the dysfunction exacerbates at older age.

Discussion

In this study, we first demonstrated that NSUN3, the enzyme required for f^5C modification of the mammalian mt-$tRNA^{Met}$ anticodon first nucleotide, is essential for embryonic development in mice (Figure 1). The first nucleotide of tRNA anticodon is responsible for proper recognition of the mRNA codon third nucleotide, and loss of NSUN3-mediated f^5C disables efficient decoding of AUA codons in mt-mRNAs[22]. Embryonic lethality of KO mice of other mt-tRNA anticodon modification enzymes, MTO1 (for τm^5U modification) and MTU1 (for 2-thiolation in τm^5s^2U modification), emphasizes the pivotal roles of mt-tRNA anticodon first nucleotide modifications in mammalian embryonic development.

Our study demonstrates that the loss of *Nsun3* leads to abnormality in heart and confirms the importance of *Nsun3* in mitochondrial function (Figures 3, 4, 6). Heart-specific *Nsun3* KO resulted in decreased mitochondrial respiratory complexes activities, fragmented mitochondrial cristae structures and mitochondrial enlargement. Interestingly, although the *Nsun3*^{HKO} heart displayed some abnormalities at young adulthood (14 weeks of age), aberrant heart phenotypes were more apparent in later adulthood (50 weeks of age). This age-exacerbated phenotype is similar to a mitochondrial $tRNA^{Met}$ mutant patient who was diagnosed as hypertension at the age of 44 and experienced thickening of left ventricle posterior wall at the age of 60s and 70s[30]. In a later report, this $tRNA^{Met}$ mutation was shown to reduce the efficiency of NSUN3-mediated $tRNA^{Met}$ modification in vitro[26]. Our work clearly indicates that deficiency of NSUN3-mediated f^5C modification in the heart is associated with heart aberrations especially at older age.

Notably, the phenotypes of *Nsun3*^{HKO} are weaker compared to the heart-specific *Mto1* KO (*Mto1*^{HKO}) mice that were previously reported[15]. *Mto1*^{HKO} mice were born, but did not survive longer than 24 hours, whereas *Nsun3*^{HKO} mice grew up to adults. The

enlargement of heart mitochondria in *Mto1*^{HKO} is more pronounced than in *Nsun3*^{HKO}. *Mto1* knockout causes cytoplasmic unfolded protein responses, due to accumulation of protein aggregates in the cytoplasm caused by impaired mitochondrial protein import from the cytoplasm[15]. By contrast, *Nsun3*^{HKO} mouse heart did not show upregulation of unfolded protein response marker mRNAs *Xbp1* or *Chop* (Supplementary Figure 3). Furthermore, while E9 embryos of whole-body *Mto1* KO or *Mtu1* KO are drastically smaller than wild-type and show aberrant morphologies[15,16], whole-body *Nsun3* KO embryos at E9.5 exhibited relatively milder phenotype with moderately smaller body size than wild-type (as shown in Supplementary Figure 4) and continued growing at least until E10.5 (Figure 1f). The differences in the severity of phenotypes between *Nsun3*, *Mto1*, and *Mtu1* knockouts may be partially attributed to the numbers of mt-tRNAs that the corresponding tRNA modifications are introduced to: NSUN3 modifies only mt-tRNA^{Met}, whereas MTO1 modifies five mt-tRNAs (mt-tRNA^{Leu1}, mt-tRNA^{Trp}, mt-tRNA^{Gln}, mt-tRNA^{Lys} and mt-tRNA^{Glu}) and MTU1 modifies three mt-tRNAs (mt-tRNA^{Gln}, mt-tRNA^{Lys} and mt-tRNA^{Glu}) [26,36]. Genetically inherited disorders caused by mt-tRNA modification deficiency are generally regarded to occur during embryonic development or at young age[3,5]. The smaller number of NSUN3-modified tRNAs compared to MTO1-modified tRNAs may be the cause of relatively mild *Nsun3*^{HKO} heart aberrations, which became more apparent in late adulthood, in contrast to the strong disorders from young ages in *Mto1*^{HKO}.

The reported human patients who have compound heterozygous mutations in the *NSUN3* gene were diagnosed to develop mitochondrial disease at several months of age[13,29]. These infants presented with symptoms of mitochondrial disease such as lactic acidosis and skeletal muscle weakness, but heart failure was not reported. On the other hand, a mt-tRNA^{Met} mutation (A4435G mutation in mtDNA) was associated with

hypertension and progressive thickening of the posterior wall of the left ventricle during his 60s and 70s, but was not associated with other clinical features[30]. This mutation site is located next to the mt-tRNA^{Met} anticodon (position 37 according to the conventional tRNA position numbering), and in vitro experiments have shown that it reduces the efficiency of NSUN3-mediated methylation to about 40%[26]. The patient with the mt-tRNA^{Met} mutation had a relatively mild phenotype compared to patients with *NSUN3* mutations, possibly due to the presence of some f^{5}C in mt-tRNA^{Met}. These previous studies and our results collectively suggest that the patients with *NSUN3* mutations should be closely monitored for potential decline in heart function as they age.

Upon *Nsun3*^{HKO}, among the five respiratory complexes, the strongest phenotypes were seen in complexes IV and I; *Nsun3*^{HKO} resulted in a decreased complex IV steady-state level and decreased complex I and IV activities in older mice, and did not substantially affect other complexes (Figure 6). One possible cause could be due to the number of AUA codons in mt-mRNAs; the numbers of mouse mt-mRNA AUA codons for each respiratory complex are 140 (complex I), 0 (complex II), 18 (complex III), 46 (complex IV) and 13 (complex V). In previous studies, similar to our *Nsun3*^{HKO} mice, knockout of mt-tRNA anticodon modification enzymes such as human *ALKBH1*, mouse *Mto1*, or mouse *Mtu1* all resulted in marked decrease in activities of respiratory complexes I and/or IV, and lesser extent or no effects on complexes II and III[15,16,37] (complex V activity cannot be measured by conventional methods). The biased effects of mt-tRNA anticodon modification enzyme knockouts to complexes I and IV may be due to the number of subunits that mt-DNA encodes; mt-DNA encodes seven subunits of complex I, no subunit of complex II, one subunit of complex III, three subunits of complex IV and two subunits of complex V.

This study does not reveal the specific mechanisms between respiratory complex dysfunction and heart abnormalities. However, previous studies have shown various mechanisms by which respiratory complex dysfunctions can lead to progressive heart deficiencies[38]. For example, dysfunction of complex IV can halt the flow of electrons from NADH via complexes I and III, inducing leakage of electrons and production of reactive oxygen species (ROS)[39]. ROS overload can directly damage tissue and also open holes in the mitochondrial inner membrane, releasing cytochrome c and triggering cell death[40]. Furthermore, deficiency in oxidative phosphorylation can cause the heart to increase glycolysis for ATP generation, leading to elevated glucose uptake into the cells. A recent study suggests that high intracellular glucose uptake can lead to accumulation of branched-chain amino acids via transcriptional rewiring, activating mTOR and causing cardiomyocyte hypertrophy[41]. It is possible that the reduced function of complex IV (Figure 6e, f) and increased glycolysis in *Nsun3*^{HKO} hearts (as suggested by the increased heart lactate level in Figure 6d) to slightly activate these pathways and result in some thickening of left ventricular posterior wall.

Previous studies have shown that the f^{5}C modification of mt-tRNA^{Met} mediated by NSUN3 plays a crucial role in maintaining the level of mitochondrial translation in human and mouse cells[13,24,26,28]. Translation levels are determined at both the initiation and elongation steps, and mt-tRNA^{Met} is used in both. An in vitro study has suggested a role for mt-tRNA^{Met} f^{5}C modification in the initiation step of translation at AUA codon and not AUG codon[42]. Additionally, f^{5}C modification was shown to enhance the efficiency of the elongation step of AUA codon translation, but had little effect on the AUG codon translation in vitro[22]. In *Nsun3*^{HKO} hearts, complex IV was the most affected respiratory complex (Figure 6), although all of the mtDNA-encoded complex IV subunit mRNAs (mt-

Co1, mt-*Co2* and mt-*Co3*) use AUG as their initiation codons (Supplementary Table 1). Thus, in the *Nsun3*^{HKO} heart, translation elongation step, rather than the initiation step, may be involved in the reduction of complex IV level.

The role of f^{5}C in the initiation of mitochondrial translation requires further studies. This is because, in addition to AUG and AUA, mammalian complex I and V mt-mRNAs also use AUU, AUC and GUG codons as initiation codons (Supplementary Table 1). Additionally, the loss of *Nsun3* loss leads to a decrease in complex I activity in *Nsun3*^{HKO} heart at an older age (Figure 6f) and a decrease in translation of mtDNA-encoded complex I, III and V proteins in human and mouse cells[26,28]. The initiation step of mitochondrial translation is different from that of bacterial or cytoplasmic translation in various ways[43]. Therefore, to understand the potential role of mt-tRNA^{Met} f^{5}C modification in translational initiation at AUU, AUC and GUG codons, it would be necessary to conduct an in vitro translation experiment that uses mitochondrial ribosomes (rather than *E. coli* ribosomes) and other mitochondrial factors.

Regarding the physiological roles of NSUN3, a lack of understanding remains of the embryonic lethal phenotype of whole-body *Nsun3* KO and relatively weak phenotype of *Nsun3*^{HKO}. Although the heart is regarded as one of the most susceptible organs to mitochondrial dysfunction at postnatal stages[31], the role of other tissues or cells for which mt-tRNA anticodon modifications play critical roles during the embryonic stage remains unclear. This question also arises with respect to the embryonic lethality of whole-body *Mto1* KO or *Mtu1* KO and viability of previously generated heart- or liver-specific *Mto1* or *Mtu1* KO mice[15,16]. Therefore, identifying the specific tissue(s) and stage(s) at which mt-tRNA modifications is critical during embryonic development will be a crucial question for mitochondrial biology and RNA biology.

Methods

Animals

Whole-body *Nsun3* knockout mice were generated by crossing transgenic mice having exon 4 of *Nsun3* gene floxed by the LoxP sequence (*Nsun3*$^{Flox/Flox}$) with transgenic mice carrying Cre recombinase under control of cytomegalovirus enhancer and chicken *β-actin* (CAG) promoter. This crossing resulted in a permanent deletion of targeted exons in the germ cells. The resulting *Nsun3*$^{(Flox/-);CAGcre}$ mice were further crossed to C57BL/6J mice to yield *Nsun3* heterozygous mice (*Nsun3*$^{+/-}$).

Heart-specific *Nsun3* knockout mice were generated by crossing transgenic mice in which the *Nsun3* gene exon 4 was floxed by LoxP sequences (*Nsun3* Flox mice), with transgenic mice expressing Cre recombinase under control of *Myh6* promoter (Myh6-Cre mice). *Nsun3* Flox mice were backcrossed with C57BL/6J mice for at least five generations to control for genetic background. Myh6-Cre mice were acquired previously[15]. Male mice were utilized for experiments, while female mice were primarily used for breeding purposes. Experiments were performed at 14 or 50 weeks of age. Mice were housed at 25°C in a 12-h light and 12-h dark cycle. All animal procedures were approved by the Animal Ethics Committee of Kumamoto University (Approval ID: A2021-012R2).

Genotyping

Genomic DNA was extracted from a 3-5 mm piece of tissue clipped from the end of the tail of 4-week-old mice. Approximately 50 ng of genomic DNA was subjected to PCR to detect the WT and KO alleles using KAPA 2G Robust HotStart ReadyMix (KAPA

Biosystems, Boston, USA), or floxed allele and Myh6-Cre alleles using KOD FX DNA polymerase (TOYOBO Life Science, Tokyo, Japan) following the manufacturer's instructions. The primers are listed in Supplementary Table 2.

Observation of embryos

Whole-body *Nsun3*$^{+/-}$ males and females were paired overnight. The next morning, males were removed from the cages. The weight of females was checked on the day before observing embryos to estimate pregnancy. To observe E12.5, E10.5 or E9.5 embryos, the female mice were euthanized by isoflurane or cervical dislocation. The uterus was quickly opened and embryos were observed in phosphate-buffered saline (PBS) under a Stemi305 stereomicroscope (Zeiss, Oberkochen, Germany).

RNA extraction

Mouse hearts were dissected and homogenized in 3 mL of TRI Reagent (MRC, Cincinnati, USA) using TissueRuptor (Qiagen, Hilden, Germany). The heart lysate in TRI Reagent was then centrifuged at 10,000 × g for 10 min, and the supernatant was used for total RNA extraction according to the manufacturer's protocol.

Reverse-transcription quantitative PCR (RT-qPCR)

RT-qPCR was performed as described previously[44]. cDNA was synthesized using 500 ng of total RNA and Prime-Script RT Master Mix (Takara, Kusatsu, Japan) according to

the manufacturer's protocol. Quantitative real-time PCR was then performed using Rotor-Gene Q MDx 5plex HRM machine (Qiagen, Hilden, Germany) and TB Green Premix Ex Taq II (Takara) according to manufacturer's instructions. The primer sequences are listed in Supplementary Table 2.

RNA nucleoside mass spectrometry

RNA nucleoside mass spectrometry was performed as previously described[45-47]. A 25 μL solution containing 3 μg of heart total RNA, 20 mM Hepes-KOH (pH 7.6), 2 units of Nuclease P1 (Fujifilm, Tokyo, Japan) and 0.25 unit of bacterial alkaline phosphatase (Takara, Kusatsu, Japan) was incubated at 37°C for 3 h. 3 μl of the nucleoside solution was then injected to the LCMS-8050 system (Shimadzu, Kyoto, Japan). The nucleosides were first separated by an Inertsil ODS-3 column (GL Science, Tokyo, Japan) using a mobile phase that continuously changed from 100% of solution A (5 mM ammonium acetate in water, pH 5.3) to 100 % of solution B (60% acetonitrile in water) in 17 min at a flow rate of 0.4 mL min^{-1}, followed by electrospray ionization and a triple quadrupole mass spectrometry in the multiple reaction monitoring mode.

Echocardiography

Mice were preconditioned by chest hair removal using a topical depilatory (FujiFilm VisualSonics, Toronto, Canada), anaesthetized with 1.5–2.5% isoflurane administered via inhalation, and maintained in a supine position on a platform with limbs attached for electrocardiogram gating during imaging. Body temperature was kept constant by

feeding the signal of a rectal probe back to a heating pad, while heart and respiratory rates were continuously monitored. Transthoracic echocardiography was performed using a high frequency ultrasound system for small animal imaging (VisualSonics Vevo 2100, FujiFilm VisualSonics, Toronto, Canada) using a MS 400 linear array transducer (18–38 MHz). M-mode recording was performed at the midventricular level. All images were analyzed using Vevo 2100 version 1.4 software. Left ventricle wall thickness and internal cavity diameters at diastole and systole were measured. Left ventricle volumes in diastolic phases (LV Vol d) and systolic phases (LV Vol s) were measured. The ejection fraction (%) was calculated as: $[(\text{LV Vol d}) - (\text{LV Vol s})]\ (\text{LV Vol d})^{-1} \times 100$. All procedures were performed under double-blind conditions with regard to genotype or treatment.

Electron microscopy

Transmission electron microscopy examination was performed essentially as described previously[48]. Briefly, heart tissues were first fixed in a solution containing 2% paraformaldehyde and 2% glutaraldehyde, cut in the fixative, and then additionally fixed at 4°C for more than 2 h. The tissues were then washed, post-fixed in 1% OsO_4 at 4°C for one hour, washed and stained with 1.5% uranyl acetate at 4°C for 1 h. After dehydration in ethanol and propylene oxide, the tissues were embedded in epoxy resin for 3 h and then polymerized at 60°C for more than 48 h. The tissues were trimmed, cut into ~60 to 70 nm sections, stained with 1.5% uranyl acetate for 10 min and with lead citrate for 10 min. Random sections were obtained from three hearts per group. Images were acquired at 80 kV on a HITACHI 7700 transmission electron microscope (Hitachi, Tokyo, Japan). The mitochondrial areas in images taken at 2500 × magnification were

quantified using ImageJ software.

Northern blot

For tRNA northern blot, total heart RNA (1.5 µg) was separated using 7 M urea/TBE/10% PAGE at 150 V. The gel was then stained with SYBR Gold (Invitrogen, Carlsbad, USA) to assess the RNA quality and then transferred to a nylon membrane (Merck Millipore, Billerica, USA) using a wet transfer blotting system (Bio-Rad, Hercules, USA) on ice at 50 V for 80 min. For mRNA northern blot, 1.8 µg of total heart RNA or 1.5 µg of RNA ladder (Nippon Gene, Tokyo, Japan) was separated using 6.7% formaldehyde/1xMOPS/1.2% agarose gel at 100 V. The RNA was then transferred to a nylon membrane (Merck Millipore, Billerica, USA) by an overnight, conventional sponging method using 20 × SSC. The next day, the membrane was briefly washed with MilliQ water, stained with methylene blue (MRC, Cincinnati, USA) and photographed. For both tRNA and mRNA northern blot, membranes were crosslinked with UV light at 1200 × 100 µJ cm^{-2} using HL-2000 Hybrilinker (Funakoshi, Tokyo, Japan) and incubated in prehybridization buffer (6 × SSC, 0.1% SDS, and 1 × Denhardt's solution) at 42°C for 1 h. The membranes were then hybridized with DIG-labeled (Roche, Basel, Switzerland) probe DNA in hybridization buffer (900 mM NaCl, 90 mM Tris-HCl pH 8, 6 mM EDTA and 0.3% SDS) overnight at 50°C. The membranes were washed with 1 × SSC, blocked using DIG wash and block buffer set (Roche), and probed with anti-DIG alkaline phosphatase Fab fragments (Roche) and CDP-Star (Roche). Images were taken by ImageQuant (GE Healthcare, Chicago, USA). Probes DNA sequences are listed in Supplementary Table 2.

Lactate level measurement

Lactate levels in mouse hearts were measured using the Lactate Colorimetric Assay Kit II (BioVision, Milpitas, USA). Each heart was homogenated in 1 mL of ice-cold lactate assay buffer in the kit using TissueRuptor (Qiagen, Hilden, Germany). The lysate was centrifuged at 10,000 × g for 5 min, and the supernatant was used for lactate measurement according to the manufacturer's protocol.

Mitochondrial fractionation

Mitochondria were isolated from fresh mouse heart tissues essentially as previously described[15,16]. Briefly, dissected heart tissue was cut into small pieces on ice with scissors and then homogenized in 5 mL of extraction buffer [225 mM mannitol, 75 mM sucrose, 10 mM HEPES-KOH (pH 7.6), 2 mM EDTA, Protease inhibitor cocktail (Roche), 0.0025% 2-mercaptoethanol] using a Teflon homogenizer with 15 strokes at 700 rpm, maintaining cooling on ice. The homogenate was centrifuged at 600 × g for 10 min at 4°C. Subsequently, the supernatant was transferred to a new tube and centrifuged at 7,000 × g for 10 min to acquire the mitochondrial fraction pellet. The mitochondrial fraction pellet was resuspended in the extraction buffer and adjusted to 1 mg mL^{-1} using a protein assay kit (Bio-Rad, Hercules, USA). The mitochondrial fraction was used for subsequent blue native PAGE and respiratory complex activity measurements.

Blue native PAGE

Blue native PAGE was performed as previously described[15]. The mitochondrial fraction containing 125 μg of protein was suspended in 40 μL of solubilizing buffer containing 50 μM bis-Tris (pH 7.0), 1 M aminocaproic acid and 1.5 % DDM (n-dodecyl β-D-maltoside). Samples were cleared by centrifuging at 100,000 × g for 15 min at 4°C. The supernatant was mixed with 3 μL of brilliant blue G (dissolved in 1 M aminocaproic acid). 20 μL of sample was subjected to blue native PAGE using a 3-12% Bis-Tris native gel (Invitrogen, Carlsbad, USA). Once the dye travelled one-third of the gel length, the first cathode buffer was replaced with the second cathode buffer (10^{-1} dilution of the first cathode buffer).

Western blot

Western blot was performed essentially as previously described[44]. Tissues were homogenized in lysis buffer (150 mM NaCl,100 mM Tris-HCl pH 8, 0.5% NP-40 and protease inhibitor cocktail (Roche, Basel, Switzerland)) and sonicated for 10 sec. The protein concentration was determined using a BCA protein assay kit (Thermo Fisher Scientific, Waltham, USA). Samples were electrophoresed in SDS polyacrylamide gel and transferred to Immobilon-P membrane (Merck Millipore, Billerica, USA). The membrane was blocked with 5% skim milk in TBST buffer (150 mM NaCl, 25 mM Tris-HCl pH 7.4, 2.7 mM KCl, 0.05% Tween-20) and probed for respective proteins using the primary antibodies diluted in 5% skim milk in TBST buffer at 4°C, overnight. The membrane was washed in TBST and was probed using the secondary antibody at room temperature for 1 h, followed by washing in TBST. The signals were detected using ECL Prime Western Blotting Detection Reagent (GE Healthcare, Chicago, USA) and an

Image Quant 400 imager (GE Healthcare). The antibodies and their conditions for use are listed in the Supplementary Table 3.

Respiratory complex activity

The mitochondrial fraction (1 mg mL^{-1}) was briefly sonicated before use and the activities of complexes I, II, III and IV were measured essentially as previously described [15,49]. For complex I activity measurement, 980 μL of solution containing 50 mM potassium phosphate (pH 7.4), 2 mM KCN, 75 μM NADH (Nicotin-amide adenine dinucleotide reduced disodium salt) and 50 μM Coenzyme Q1, was mixed and incubated at 30°C for 3 min. Subsequently, 20 μL (20 μg) of mitochondrial protein was added and absorbance at 340 nm was measured for 200 seconds. Enzymatic activity was calculated using the extinction coefficient of NADH (6.22 mM^{-1} cm^{-1}).

For complex II activity measurement, 965 μL of reaction solution containing 50 mM potassium phosphate (pH 7.4), 20 mM succinate and 20 μg of mitochondrial protein was mixed and incubated at 30°C for 10 min. Subsequently, final concentrations of 2 μg mL^{-1} of Antimycin A, 2 μg mL^{-1} of rotenone, 2 mM KCN, 50 μM DCPIP (2,6-Dichloroindophenol sodium salt hydrate) and DB (decylubiquinone) were added and absorbance at 600 nm was measured for 200 seconds. Enzymatic activity was calculated using the extinction coefficient of DCPIP (19.1 mM^{-1} cm^{-1}).

Prior to complex III activity measurement, we prepared DBH_2 solution by mixing 100 μL of DB with 10 mg of potassium borohydride and 10 μL of 100 mM HCl. The supernatant was transferred to a new tube and 5 μL of 1 M HCl was added. For complex III activity measurement, 984 μL of reaction solution containing 10 mM potassium

phosphate (pH 7.4), 50 μM cytochrome C, 1 mM EDTA, 2 mM KCN and 4 μM rotenone was mixed and incubated at 30°C for 10 min. Subsequently, 10 μg (10 μL) of mitochondrial protein and 6 μL of DBH_2 solution were added and absorbance at 550 nm was measured for 200 seconds. Enzymatic activity was calculated using the extinction coefficient of cytochrome c (19.0 mM^{-1} cm^{-1}).

Prior to complex IV activity measurement, 2.7 mg of cytochrome c was dissolved in MilliQ water and 5 μL of 100 mM dithiothreitol was added and incubated for >15 min at room temperature in the dark. For complex IV activity measurement, 1 mL of reaction solution containing 10 mM potassium phosphate (pH 7.4), 50 μL of cytochrome c and 10 μL (10 μg) of mitochondrial proteins was mixed and absorbance at 550 nm measured for 200 seconds. Enzymatic activity was calculated using the extinction coefficient of cytochrome c (19.0 mM^{-1} cm^{-1}).

For citrate synthase activity measurement, 1 mL of reaction solution containing 100 mM Tris-HCl (pH 8.0), 300 mM acetyl-coA, 0.1 mM DTNB (5,5'-dithiobis 2-nitrobenzoic acid), 0.5 mM oxaloacetate, and 10 μL (10 μg) of mitochondrial proteins were mixed and absorbance at 412 nm measured for 200 seconds. Enzymatic activity was calculated using the extinction coefficient of TNB (thionitrobenzoic acid) (13.6 mM^{-1} cm^{-1}).

Statistics and reproducibility

All numerical data were analyzed by GraphPad Prism 9 software. All the 'n' corresponds to individual animals. Three to five animals were used for each group to confirm reproducibility and minimize animal sacrifice. No data were excluded. Control and KO

animals were tested in the order of Control 1, KO1, Control 2, KO2, Control 3, KO3, ... unless otherwise noted to minimize time bias in experiments. Blinding was not performed unless otherwise noted, due to constraints of time and personnel. To assess differences between two groups, Welch's *t*-test was used unless otherwise noted. A two-tailed *P* value of 0.05 was considered significant. To assess differences between four groups with two variables, two-way analysis of variance (ANOVA) followed by Tukey's test was used. Data are presented as means ± standard error of means (s.e.m.).

References

1 Crick, F. On protein synthesis. *Symp Soc Exp Biol* **12**, 138-163 (1958).

2 Hoagland, M. B., Stephenson, M. L., Scott, J. F., Hecht, L. I. & Zamecnik, P. C. A soluble ribonucleic acid intermediate in protein synthesis. *J Biol Chem* **231**, 241-257 (1958).

3 Chujo, T. & Tomizawa, K. Human transfer RNA modopathies: diseases caused by aberrations in transfer RNA modifications. *FEBS J* **288**, 7096-7122, doi:10.1111/febs.15736 (2021).

4 Suzuki, T. The expanding world of tRNA modifications and their disease relevance. *Nat Rev Mol Cell Biol* **22**, 375-392, doi:10.1038/s41580-021-00342-0 (2021).

5 de Crecy-Lagard, V. *et al.* Matching tRNA modifications in humans to their known and predicted enzymes. *Nucleic Acids Res* **47**, 2143-2159, doi:10.1093/nar/gkz011 (2019).

6 Anderson, S. *et al.* Sequence and organization of the human mitochondrial genome. *Nature* **290**, 457-465, doi:10.1038/290457a0 (1981).

7 Suzuki, T. *et al.* Complete chemical structures of human mitochondrial tRNAs. *Nat Commun* **11**, 4269, doi:10.1038/s41467-020-18068-6 (2020).

8 Ghezzi, D. *et al.* Mutations of the mitochondrial-tRNA modifier MTO1 cause hypertrophic cardiomyopathy and lactic acidosis. *Am J Hum Genet* **90**, 1079-1087, doi:10.1016/j.ajhg.2012.04.011 (2012).

9 Kopajtich, R. *et al.* Mutations in GTPBP3 cause a mitochondrial translation defect associated with hypertrophic cardiomyopathy, lactic acidosis, and encephalopathy. *Am J Hum Genet* **95**, 708-720, doi:10.1016/j.ajhg.2014.10.017 (2014).

10 Metodiev, M. D. *et al.* Recessive Mutations in TRMT10C Cause Defects in Mitochondrial RNA Processing and Multiple Respiratory Chain Deficiencies. *Am J Hum Genet* **98**, 993-1000, doi:10.1016/j.ajhg.2016.03.010 (2016).

11 Patton, J. R., Bykhovskaya, Y., Mengesha, E., Bertolotto, C. & Fischel-Ghodsian, N. Mitochondrial myopathy and sideroblastic anemia (MLASA): missense mutation in the pseudouridine synthase 1 (PUS1) gene is associated with the loss of tRNA pseudouridylation. *J Biol Chem* **280**, 19823-19828, doi:10.1074/jbc.M500216200 (2005).

12 Powell, C. A. *et al.* TRMT5 mutations cause a defect in post-transcriptional modification of mitochondrial tRNA associated with multiple respiratory-chain deficiencies. *Am J Hum Genet* **97**, 319-328, doi:10.1016/j.ajhg.2015.06.011 (2015).

13 Van Haute, L. *et al.* Deficient methylation and formylation of mt-tRNA(Met) wobble cytosine in a patient carrying mutations in NSUN3. *Nat Commun* **7**, 12039, doi:10.1038/ncomms12039 (2016).

14 Zeharia, A. *et al.* Acute infantile liver failure due to mutations in the TRMU gene. *Am J Hum Genet* **85**, 401-407, doi:10.1016/j.ajhg.2009.08.004 (2009).

15 Fakruddin, M. *et al.* Defective mitochondrial tRNA taurine modification activates global proteostress and leads to mitochondrial disease. *Cell Rep* **22**, 482-496, doi:10.1016/j.celrep.2017.12.051 (2018).

16 Wu, Y. *et al.* Mtu1-Mediated Thiouridine Formation of Mitochondrial tRNAs Is Required for Mitochondrial Translation and Is Involved in Reversible Infantile Liver Injury. *PLoS Genet* **12**, e1006355, doi:10.1371/journal.pgen.1006355 (2016).

17 Wei, F. Y. *et al.* Cdk5rap1-mediated 2-methylthio modification of mitochondrial tRNAs governs protein translation and contributes to myopathy in mice and humans. *Cell Metab* **21**, 428-442, doi:10.1016/j.cmet.2015.01.019 (2015).

18 Shinoda, S. *et al.* Mammalian NSUN2 introduces 5-methylcytidines into mitochondrial tRNAs. *Nucleic Acids Res* **47**, 8734-8745, doi:10.1093/nar/gkz575 (2019).

19 Tuorto, F. *et al.* RNA cytosine methylation by Dnmt2 and NSun2 promotes tRNA stability and protein synthesis. *Nat Struct Mol Biol* **19**, 900-905, doi:10.1038/nsmb.2357 (2012).

20 Blanco, S. *et al.* Aberrant methylation of tRNAs links cellular stress to neuro-developmental disorders. *EMBO J* **33**, 2020-2039, doi:10.15252/embj.201489282 (2014).

21 Moriya, J. *et al.* A novel nucleoside found at the first position of the anticodon of methionine tRNA from bovine liver mitochondria. *Biochemistry* **33**, 2234-2239, doi:10.1021/bi00174a033, (1994).

22 Takemoto, C. *et al.* Unconventional decoding of the AUA codon as methionine by mitochondrial tRNAMet with the anticodon f5CAU as revealed with a mitochondrial in vitro translation system. *Nucleic Acids Res* **37**, 1616-1627, doi:10.1093/nar/gkp001 (2009).

23 Cantara, W. A., Murphy, F. V. t., Demirci, H. & Agris, P. F. Expanded use of sense codons is regulated by modified cytidines in tRNA. *Proc Natl Acad Sci U S A* **110**, 10964-10969, doi:10.1073/pnas.1222641110 (2013).

24 Haag, S. *et al.* NSUN3 and ABH1 modify the wobble position of mt-tRNAMet to expand codon recognition in mitochondrial translation. *EMBO J* **35**, 2104-2119, doi:10.15252/embj.201694885 (2016).

25 Kawarada, L. *et al.* ALKBH1 is an RNA dioxygenase responsible for cytoplasmic and

mitochondrial tRNA modifications. *Nucleic Acids Res* **45**, 7401-7415, doi:10.1093/nar/gkx354 (2017).

26 Nakano, S. *et al.* NSUN3 methylase initiates 5-formylcytidine biogenesis in human mitochondrial tRNA(Met). *Nat Chem Biol* **12**, 546-551, doi:10.1038/nchembio.2099 (2016).

27 Rath, S. *et al.* MitoCarta3.0: an updated mitochondrial proteome now with sub-organelle localization and pathway annotations. *Nucleic Acids Res* **49**, D1541-D1547, doi:10.1093/nar/gkaa1011 (2021).

28 Trixl, L. *et al.* RNA cytosine methyltransferase Nsun3 regulates embryonic stem cell differentiation by promoting mitochondrial activity. *Cell Mol Life Sci* **75**, 1483-1497, doi:10.1007/s00018-017-2700-0 (2018).

29 Paramasivam, A., Meena, A. K., Venkatapathi, C., Pitceathly, R. D. S. & Thangaraj, K. Novel Biallelic NSUN3 Variants Cause Early-Onset Mitochondrial Encephalomyopathy and Seizures. *J Mol Neurosci* **70**, 1962-1965, doi:10.1007/s12031-020-01595-8 (2020).

30 Liu, Y. *et al.* Mitochondrial transfer RNAMet 4435A>G mutation is associated with maternally inherited hypertension in a Chinese pedigree. *Hypertension* **53**, 1083-1090, doi:10.1161/HYPERTENSIONAHA.109.128702 (2009).

31 DiMauro, S. & Schon, E. A. Mitochondrial respiratory-chain diseases. *N Engl J Med* **348**, 2656-2668, doi:10.1056/NEJMra022567 (2003).

32 Garcia, D. & Shaw, R. J. AMPK: Mechanisms of cellular energy sensing and restoration of metabolic balance. *Mol Cell* **66**, 789-800, doi:10.1016/j.molcel.2017.05.032 (2017).

33 Westermann, B. Bioenergetic role of mitochondrial fusion and fission. *Biochim Biophys Acta* **1817**, 1833-1838, doi:10.1016/j.bbabio.2012.02.033 (2012).

34 Ojala, D., Montoya, J. & Attardi, G. tRNA punctuation model of RNA processing in human mitochondria. *Nature* **290**, 470-474, doi:10.1038/290470a0 (1981).

35 Chujo, T. *et al.* LRPPRC/SLIRP suppresses PNPase-mediated mRNA decay and promotes polyadenylation in human mitochondria. *Nucleic Acids Res* **40**, 8033-8047, doi:10.1093/nar/gks506 (2012).

36 Suzuki, T., Nagao, A. & Suzuki, T. Human mitochondrial tRNAs: biogenesis, function, structural aspects, and diseases. *Annu Rev Genet* **45**, 299-329, doi:10.1146/annurev-genet-110410-132531 (2011).

37 Asano, K. *et al.* Metabolic and chemical regulation of tRNA modification associated with taurine deficiency and human disease. *Nucleic Acids Res* **46**, 1565-1583, doi:10.1093/nar/gky068 (2018).

38 Zhou, B. & Tian, R. Mitochondrial dysfunction in pathophysiology of heart failure. *J Clin Invest* **128**, 3716-3726, doi:10.1172/JCI120849 (2018).

39 Kadenbach, B. Complex IV - The regulatory center of mitochondrial oxidative phosphorylation. *Mitochondrion* **58**, 296-302, doi:10.1016/j.mito.2020.10.004 (2021).

40 Bernardi, P. & Di Lisa, F. The mitochondrial permeability transition pore: molecular nature and role as a target in cardioprotection. *J Mol Cell Cardiol* **78**, 100-106, doi:10.1016/j.yjmcc.2014.09.023 (2015).

41 Shao, D. *et al.* Glucose promotes cell growth by suppressing branched-chain amino acid degradation. *Nat Commun* **9**, 2935, doi:10.1038/s41467-018-05362-7 (2018).

42 Bilbille, Y. *et al.* The human mitochondrial tRNAMet: structure/function relationship of a unique modification in the decoding of unconventional codons. *J Mol Biol* **406**, 257-274, doi:10.1016/j.jmb.2010.11.042 (2011).

43 Ayyub, S. A. & Varshney, U. Translation initiation in mammalian mitochondria- a prokaryotic perspective. *RNA Biol* **17**, 165-175, doi:10.1080/15476286.2019.1690099 (2020).

44 Takesue, Y. *et al.* Regulation of growth hormone biosynthesis by Cdk5 regulatory subunit associated protein 1-like 1 (CDKAL1) in pituitary adenomas. *Endocr J* **66**, 807-816, doi:10.1507/endocrj.EJ18-0536 (2019).

45 Hirayama, M. *et al.* FTO Demethylates Cyclin D1 mRNA and Controls Cell-Cycle Progression. *Cell Rep* **31**, 107464, doi:10.1016/j.celrep.2020.03.028 (2020).

46 Nagayoshi, Y. *et al.* Loss of Ftsj1 perturbs codon-specific translation efficiency in the brain and is associated with X-linked intellectual disability. *Sci Adv* **7**, doi:10.1126/sciadv.abf3072 (2021).

47 Nagayoshi, Y. *et al.* t(6)A and ms(2)t(6)A Modified Nucleosides in Serum and Urine as Strong Candidate Biomarkers of COVID-19 Infection and Severity. *Biomolecules* **12**, doi:10.3390/biom12091233 (2022).

48 Wei, F. Y. *et al.* Deficit of tRNA(Lys) modification by Cdkal1 causes the development of type 2 diabetes in mice. *J Clin Invest* **121**, 3598-3608, doi:10.1172/JCI58056 (2011).

49 Trounce, A., Kim, Y., Jun, A. & Wallace, D. Assessment of mitochondrial oxidative phosphorylation in patient muscle biopsies, lymphoblasts, and transmitochondrial cell lines. *Methods Enzymol* **264**, 484-509 (1996).

50 Suzuki, T. & Suzuki, T. A complete landscape of post-transcriptional modifications in mammalian mitochondrial tRNAs. *Nucleic Acids Res* **42**, 7346-7357, doi:10.1093/nar/gku390 (2014).

51 Steinberg, S., Misch, A. & Sprinzl, M. Compilation of tRNA sequences and sequences of tRNA genes. *Nucleic Acids Res* **21**, 3011-3015 (1993).

Acknowledgements

We thank the members of the Tomizawa lab and Tsutomu Suzuki (University of Tokyo) for fruitful discussions, Yuka Tashiro, Nobuko Maeda and Tetsuya Watanabe for technical assistance, Natalie DeWitt for critical reading and language editing and ChatGPT for language editing. Electron microscopy analysis was performed at the International Core-facility of Advanced Science in Kumamoto University. This study was supported by Japan Society for the Promotion of Science KAKENHI [18H02865 and 17KT0054 to KT, 18H02599 and 21H05265 to FYW, 20H03187 and 21K19234 to TC], Cooperative Research Project Program of Joint Usage/Research Center at the Institute of Development, Aging and Cancer, Tohoku University (to TC), and Fusion Oriented Research for Disruptive Science and Technology [JPMJFR204Z to TC].

Author contributions

YM performed most experiments. HH, YM and FYW performed cardiac ultrasonography experiments. YM, TC, YK, K. Miyata and TK analyzed embryos. TC performed northern blot and lactate assay. FYW and KT conceived the study. YM, FYW and TC designed experiments. TC, FYW, KT, K. Miura, YA, YO and MU supervised the study. TC, FYW, KT and YM wrote the manuscript.

Competing interests

The authors declare no competing interests.

Data availability

All data presented in this study are available upon request.

Figure legends

Figure 1. Embryonic lethality of whole-body *Nsun3* KO mice. a) Secondary structure of the mouse mitochondrial (mt-) $tRNA^{Met}$ with modified nucleosides: pseudouridine (Ψ) and 5-formylcytidine (f^5C). The modifications are depicted based on human and bovine mt-$tRNA^{Met}$ modifications[7,50]. The nucleoside position is numbered following conventional guidelines[51]. Note that f^5CAU anticodon can base pair with two mitochondrial methionine-encoding mRNA codons AUG and AUA. **b)** Chemical structure of f^5C. The formyl modification at cytidine *C5* position is shown in red. **c)** Numbers of animals obtained by crossing parental heterozygous (*Nsun3* +/-) mice. *P*-value was calculated by chi square test. **d)** Genotyping analysis of embryos at stage E12.5. **e, f)** Morphology of WT (+/+), heterozygous (+/-) and KO (-/-) embryos at stages E12.5 (**e**) and E10.5 (**f**) removed from the uterus of a heterozygous mother mouse. Scale bars, 5 mm (**e**) and 1 mm (**f**).

Figure 2. Generation of heart-specific *Nsun3* knockout (*Nsun3*^{HKO}) mice. a) Schematic illustration of the strategy to generate *Nsun3*^{HKO} mice. **b)** Body weight of Flox mice and *Nsun3*^{HKO} mice at the time of sacrifice (13-20 weeks). Means ± s.e.m. from n = 4 mice. n.s., not significant by Welch's *t*-test. **c)** RT-qPCR of *Nsun3* mRNA exon 3 - exon 4 using heart total RNA of 50-week-old Flox mice and *Nsun3*^{HKO} mice. The values were normalized by *Actb* mRNA levels. a.u., arbitrary units. Means ± s.e.m. from n = 4 mice. **d)** LC-MS analysis of total RNA nucleosides made by nuclease P1 digestion of total RNA from mouse heart. Mass chromatograms detecting multiple reaction monitoring of f^5C (Q1/Q3 = 272.20/140.20) or 2'-*O*-methylcytidine (Cm, a loading control,

Q1/Q3 = 258.25/112.05) are shown. Q1/Q3: the mass of the single-protonated precursor ion and product ion.

Figure 3. Heart aberrations in *Nsun3*^{HKO} mice. a) The mass of 14- and 50-week-old mice hearts that were dissected and measured after echocardiography. **b)** Representative M-mode echocardiography images of 50-week-old Flox mice and *Nsun3*^{HKO} mice. Upper images show the axis view of the left ventricle. Lower panels show the M-mode trancing of the left ventricle. **c)** Schematic of diastolic stage and systolic stage of heart. **d)** Left ventricle relative mass estimated by the echocardiography image analysis. **e)** Left ventricle volume at diastolic stage (left panel) and systolic stage (right panel). **f)** Calculated ejection fraction (%) of the hearts. **g)** Left ventricle posterior wall thickness at diastolic stage (left panel) and systolic stage (right panel). Means ± s.e.m. from n = 3 mice (14-week-old Flox) or 4 mice (14-week-old *Nsun3*^{HKO}, 50-week-old Flox and *Nsun3*^{HKO} mice). $^{**}P < 0.01$, $^{*}P < 0.05$ by two-way ANOVA followed by Tukey's test.

Figure 4. Morphological abnormalities of *Nsun3*^{HKO} mouse heart mitochondria. a, b) Representative images of mitochondria in cardiac muscles of 50-week-old Flox mice (**a**) and *Nsun3*^{HKO} mice (**b**). Scale bar, 1 μm. **c)** Histogram showing the size distribution of cardiac mitochondria from 14- or 50-week-old, Flox or *Nsun3*^{HKO} mice. n = 300 mitochondria in each group were analyzed. **d)** Violin plot of the same data as shown in the histogram. The mean mitochondrial areas (Flox 14-wk, 0.690 μm^2; HKO 14-wk, 1.011 μm^2; Flox 50-wk, 0.685 μm^2; HKO 50-wk, 1,174 μm^2) are indicated by horizontal lines. $^{****}P < 0.0001$, $^{*}P < 0.05$ by Mann Whitney test.

Figure 5. The steady-state levels of mt-tRNAs and mt-mRNAs in *Nsun3*^{HKO} mouse heart.

a) Schematic of the linearized mtDNA structure consisted of tRNA genes (yellow), protein-coding genes (blue), rRNA genes (orange) and noncoding regions (grey). Polycistronic precursor RNAs are transcribed from the heavy-strand promoter (HSP) and light-strand promoter (LSP), followed by cleavages at the 5' and 3' sides of tRNAs to produce respective RNAs. The *mt-tRNA*^{Met} gene is indicated in red, and genes encoding northern blotted RNAs are indicated in bold letters. **b)** Northern blot analysis of heart tRNAs from 14-week-old, n = 4 Flox and *Nsun3*^{HKO} mice. Cytoplasmic 5.8S rRNA is shown as a loading control, and cytoplasmic tRNA$^{Leu}_{CAA}$ is shown as a comparison to mt-tRNAs. **c**) Quantification of tRNAs in (**b**) and mt-mRNAs in (**d**) and (**e**). tRNA was normalized by 5.8S rRNA, and mRNA was normalized by 28S rRNA. Means ± s.e.m. from n = 4 Flox and *Nsun3*^{HKO} mice. ****$P < 0.0001$, ***$P < 0.001$, **$P < 0.01$, *$P < 0.05$ by Welch's *t*-test. **d**) Northern blot analysis of heart mt-*Nd2* mRNA from the same mice used in tRNA analysis. Mature mt-*Nd2* mRNA is 1038 nt plus poly(A) tail of up to 50 nt. The methylene blue-stained membrane used for mt-*Nd2* mRNA northern blot is shown on the right to monitor RNA transfer. M indicates size marker. **e**) Northern blot analysis of heart mt-mRNAs from the same mice as in above analyses. All of the mtDNA-encoded complex IV subunit mRNAs (mt-*Co1*, mt-*Co2*, mt-*Co3*) were monitored.

Figure 6. Dysfunction of specific respiratory complexes in *Nsun3*^{HKO} mouse heart.

a, b) Blue native-PAGE of respiratory complexes of 14-week-old (**a**) and 50-week-old (**b**) mouse heart mitochondria. **c)** Western blot analysis of complexes I-V proteins in 50-

week-old mice hearts. mtDNA-encoded MT-CO1 is shown in green and nuclear DNA-encoded proteins in blue. VDAC1 is a loading control of mitochondrial lysate. **d)** Relative lactate levels in the hearts of 14-week-old mice. Means ± s.e.m. from n = 5 mice each. ***P < 0.001 by Welch's *t*-test. **e, f)** Relative activities of respiratory complexes I-IV in 14-week-old (**e**) and 50-week-old (**f**) mice heart mitochondria. CS, citrate synthase activity, measured as a loading control. Means ± s.e.m. from n = 3 mice (14-week-old Flox) or 4 mice (14-week-old *Nsun3*^{HKO}, 50-week-old, Flox or *Nsun3*^{HKO} mice). **P < 0.01 by Welch's *t*-test.

Figure 1. Embryonic lethality of whole-body *Nsun3* KO mice.

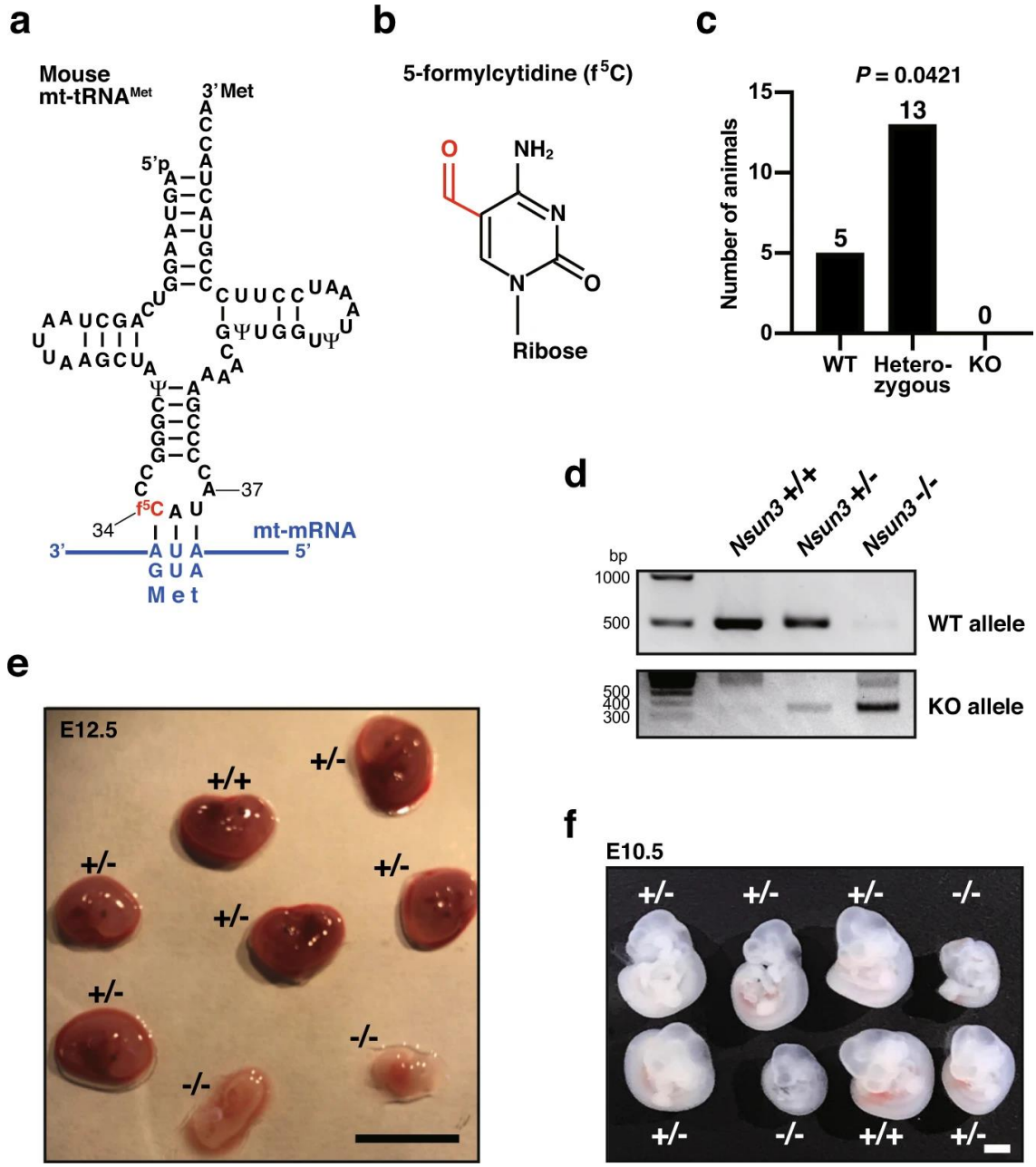

Figure 2. Generation of heart-specific *Nsun3* knockout (*Nsun3*^{HKO}) mice.

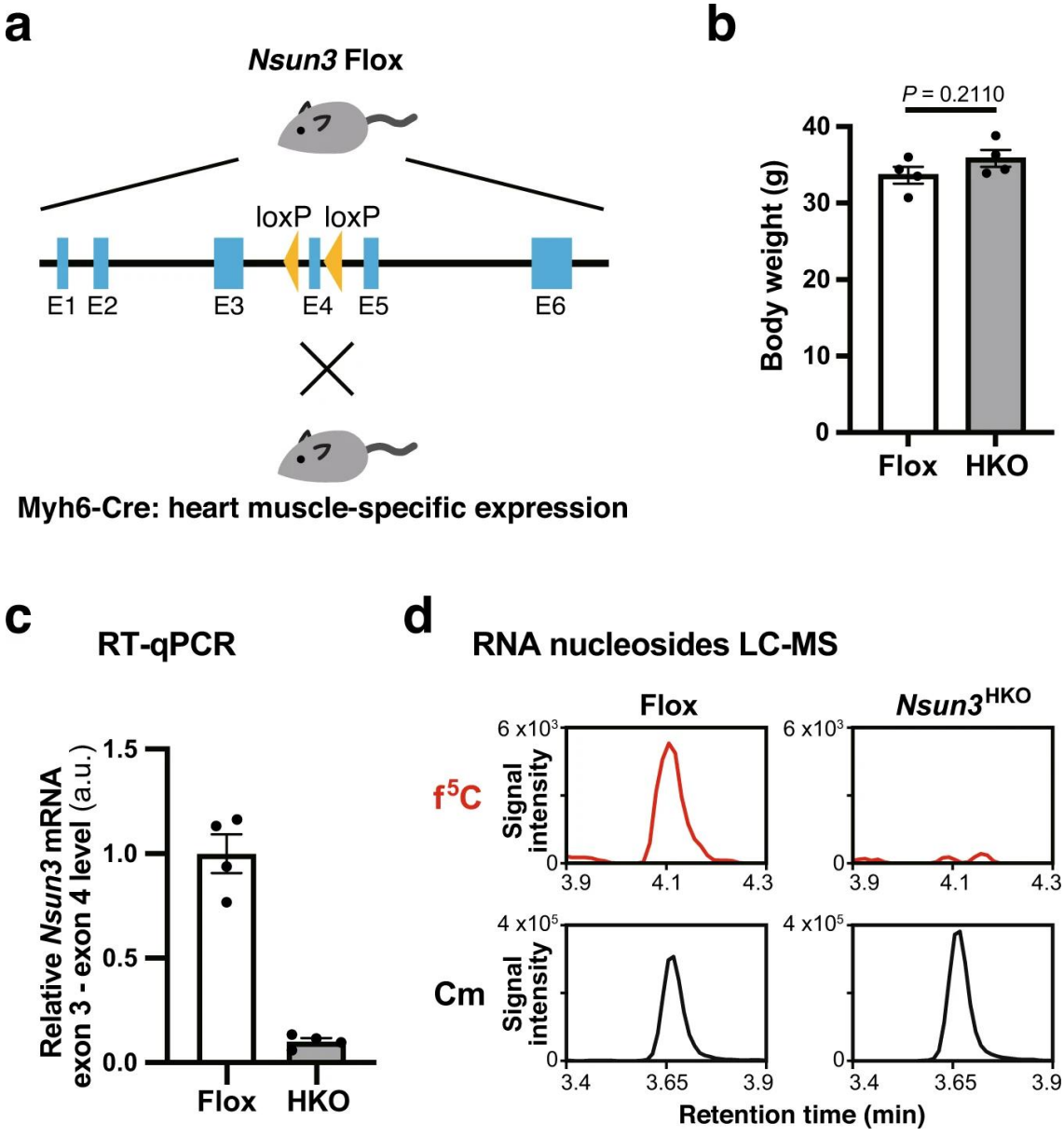

Figure 3. Heart aberrations in *Nsun3*^{HKO} mice.

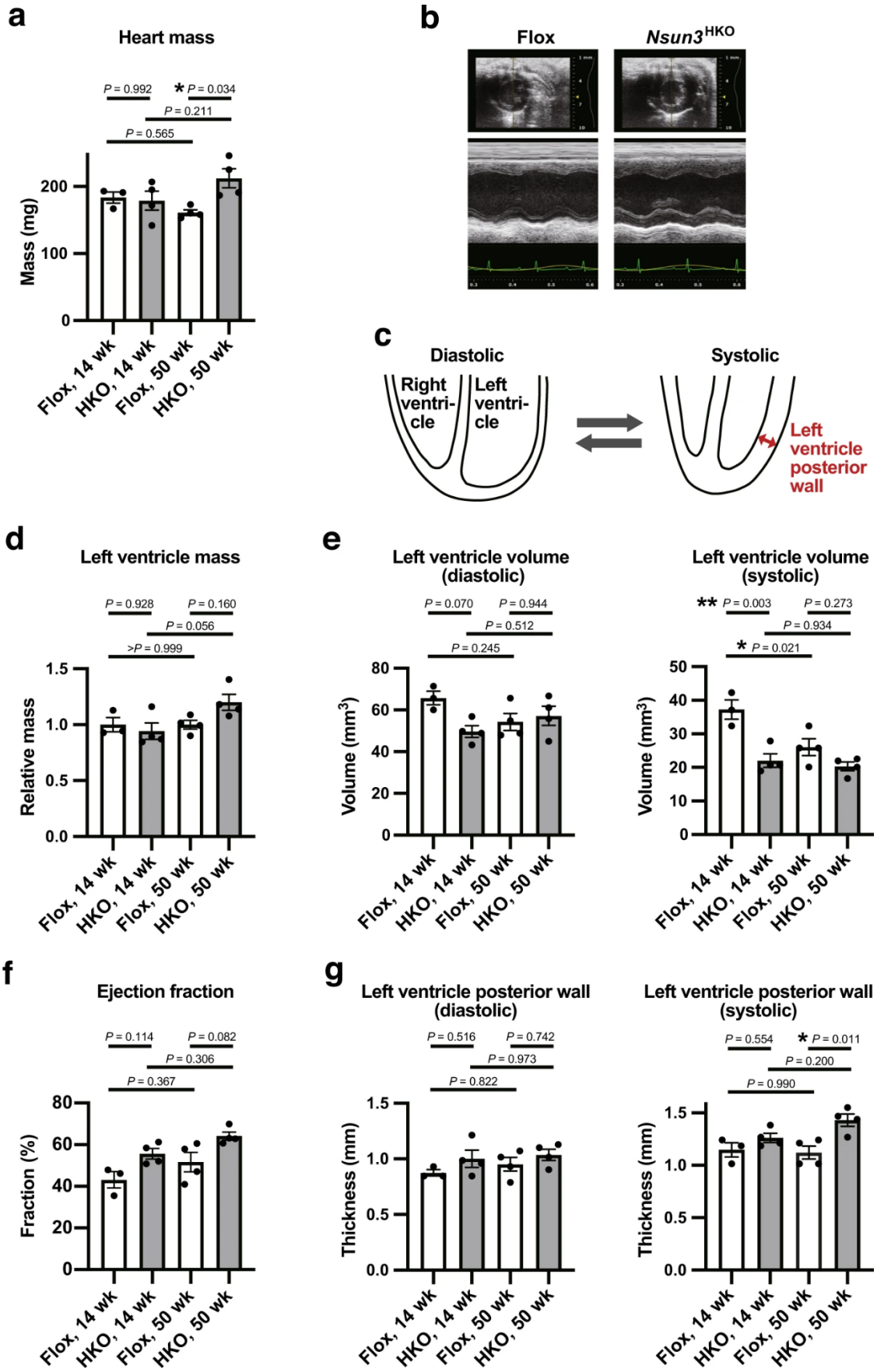

Figure 4. Morphological abnormalities of *Nsun3*^{HKO} mouse heart mitochondria.

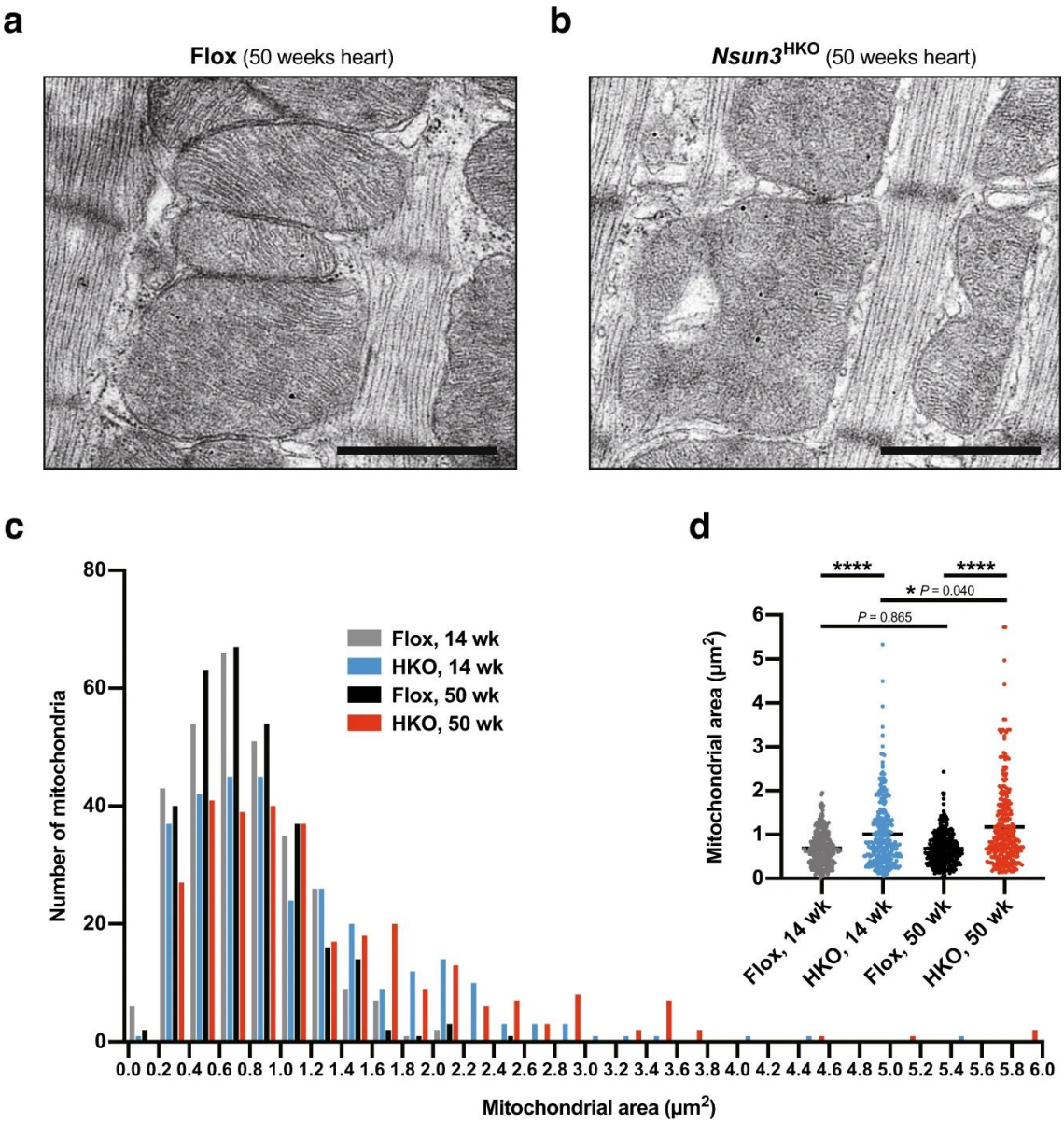

Figure 5. The steady-state levels of mt-tRNAs and mt-mRNAs in *Nsun3*^{HKO} mouse heart.

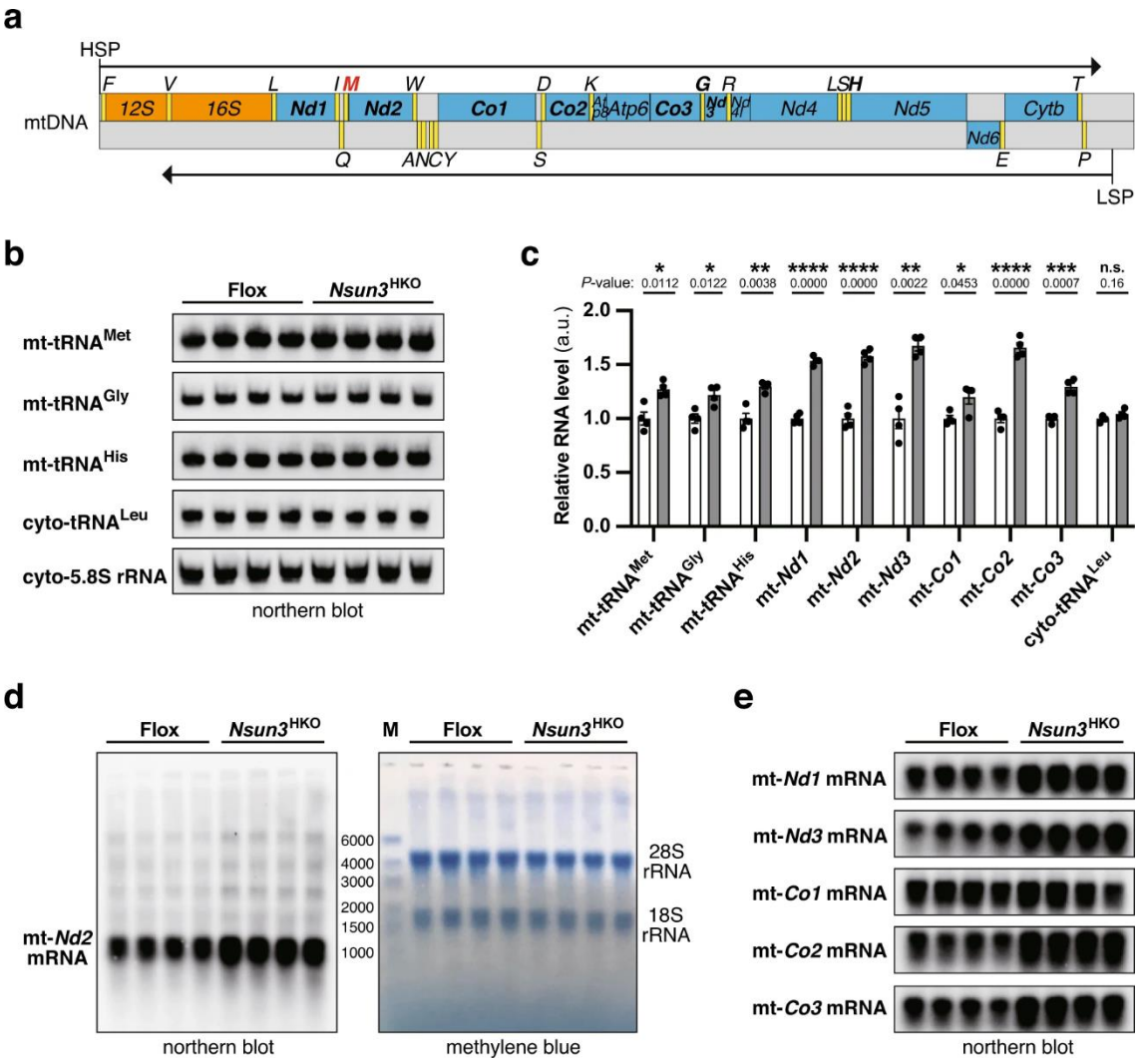

Figure 6. Dysfunction of specific respiratory complexes in *Nsun3*^{HKO} mouse heart.